Results in Physics 21 (2021) 103843

Contents lists available at ScienceDirect

Results in Physics

journal homepage: www.elsevier.com/locate/rinp

Near zero thermal expansion in metal matrix composites based on intermediate valence systems: Al/SmB_6

D.A. Serebrennikov [a,*], A.A. Bykov [b], A.L. Trigub [c], N.A. Kolyshkin [c], A.L. Freydman [d,e], A. V. Aborkin [f], A.O. Tovpinets [a], E.S. Clementyev [a], A.Yu. Goikhman [a]

[a] REC "Functional Nanomaterials", Immanuel Kant Baltic Federal University, 236016 Kaliningrad, Russia
[b] Petersburg Nuclear Physics Institute, 188300 Gatchina, Russia
[c] NRC «Kurchatov Institute», 123182 Moscow, Russia
[d] Kirensky Institute of Physics, Federal Research Center KSC SB RAS, 660036 Krasnoyarsk, Russia
[e] Siberian Federal University, 660041 Krasnoyarsk, Russia
[f] Vladimir State University, 600000 Vladimir, Russia

ARTICLE INFO

Keywords:
Metal-matrix composites (MMCs)
Intermediate valence systems
Negative thermal expansion
Invar alloys

ABSTRACT

This work is focused on the fabrication and characterization of a new type of composite invar materials combining near-zero thermal expansion and functional properties that are important for applications. This is accomplished through the use of particles of SmB_6, an intermediate valence system with negative thermal expansion, embedded in Al matrix. The composite based on SmB_6-21 vol% was fabricated by hot pressing and was characterized by XRD, optical/electron microscopy, X-ray computed tomography and capacitive dilatometry. The study of thermal expansion revealed that the sample exhibits invar behaviour up to ~60 K with a zero value of the coefficient of thermal expansion near 45 K. In comparison to pure aluminum, the temperature range has increased by about 20 K. A quantitative analysis of dilatometric experimental data performed on the basis of widely used theoretical models showed that the thermal expansion of the Al/SmB_6 composite was well reproduced within the Turner model.

Introduction

The discovery of invar alloys has led to significant progress in the development of high precision instruments such as mechanical chronometers, metrology devices, valves in engines, etc. Although invar is a registered trade name of Fe-Ni36 alloy, invar behaviour, i.e. extremely low coefficient of thermal expansion (CTE), is not bound to that system alone [1–3]. Classical Fe-based invar alloys exhibit reduced thermal expansion in the magnetically ordered domain below Curie-temperature, while in the paramagnetic state "normal" thermal expansion is recovered [2]. Using *ab initio* calculations, Schilfgaarde et al. showed that the anomalous contribution to thermal expansion of iron-nickel alloys results from the relaxation of magnetic structures, in which spins may be canted with respect to the average magnetization direction [4]. Despite the low CTE, Fe-Ni36 alloy does not possess many physical properties essential for applications [5]. At the same time, relatively high CTE values are a common property of the majority of metallic functional materials [6]. To reduce the high thermal expansion of functional materials, metal matrix composites (MMCs) reinforced with various ceramic particles were developed [7–10]. Reinforcement materials include carbides (e.g., SiC, B_4C), nitrides (e.g., Si_3N_4), oxides (e.g., A_2O_3, SiO_2) and several others [11]. A major step towards controllable thermal expansion in MMCs was made by the discovery of isotropic negative thermal expansion (NTE) over a wide temperature range in ZrW_2O_8 [12]. NTE fillers such as ZrW_2O_8, $Sc_2W_3O_{12}$, $Y_2W_3O_{12}$, which contract upon heating, have been promising candidates for the materials intended to compensate for the positive thermal expansion of functional materials [13–15]. Anomalous NTE in zirconium tungstate and related compounds is driven by coupled rotations of rigid polyhedral units ZrO_6 and WO_4 [12,16]. In the meantime, a large number of NTE materials, in which the underlying reasons for this anomalous behaviour are fundamentally different, have been found. All principal mechanisms of NTE have been well described in the review articles [17–20].

In searching for compounds with a highly anomalous contribution to thermal expansion we should explore the systems, in which the lattice

* Corresponding author.
E-mail address: dimafania@mail.ru (D.A. Serebrennikov).

https://doi.org/10.1016/j.rinp.2021.103843
Received 23 October 2020; Received in revised form 3 January 2021; Accepted 11 January 2021
Available online 16 January 2021

Table 1
NTE values of selected IV systems.

Materials	NTE temperature range, K	Minimum CTE value, $\times 10^{-6}$ K^{-1}	Reference
$Sm_{0.8}B_6$	5–90	−4	[22]
SmB_6	10–130	−4.2	[22]
$Sm_{0.9}La_{0.1}B_6$	55–156	−3.1	[22]
$Sm_{0.78}La_{0.22}B_6$	20–200	−3.1	[26]
$Sm_{0.5}La_{0.5}B_6$	10–160	−1.3	[26]
$Sm_{2.75}C_{60}$	4–32	−400	[24]
$Yb_{2.75}C_{60}$	0–60	−550	[28]
$Sm_{0.67}Y_{0.33}S$	5–250	−57	[23]
$Sm_{0.55}Y_{0.45}S$	20–250	−53	[23]
fcc-Pr	575–720	−37.5	[29]
$YbCu_4Ag$	0–50	−8	[30]
YbCuAl	0–240	−15	[31]
$YbCu_2Si_2$	5–55	−4	[32]

shrinkage is induced by transformations of electron configurations. This class of materials includes intermediate valence (IV) systems – unique chemical compounds based on the 4*f*-elements with partially filled, almost localized configurations that are nearly degenerate [21]. The effective size of rare earth ions is strongly affected by the temperature-induced changes in the partial delocalization of the 4f electron shell. Thus, NTE is observed in IV systems, in which the thermally excited state of rare earth ions has a lower atomic volume. Samarium-based IV compounds, such as SmB_6, $Sm_{1-x}(Y_x)S$, $Sm_{2.75}C_{60}$, may serve as illustrative examples [22–24]. In these systems samarium has two competing electronic configurations: a non-magnetic Sm^{2+} with the $4f^6$ configuration ($J = 0$, the main term is $^7F_0$) and magnetic Sm^{3+} with the $4f^5$ configuration ($J = 5/2$, the main term is $^6H_{5/2}$). Since the appearance of an additional electron on the 4f shell effectively shields nuclear charge for outer electrons, the effective size of Sm^{2+} is much larger than that of Sm^{3+}. The greater the partial charge transfer between the two electronic configurations, the larger the anomalous contribution to thermal expansion is. This specific feature may be a key to controllable thermal expansion. It is possible to tune the overall thermal expansion of the material, provided that there is a way to adjust the magnitude and the temperature scale of the charge transfer between the two electronic states in the system. Sm-based IV systems are prone to demonstrate tunable effective valence of samarium ions caused either by introducing vacancies in the rare-earth sublattice or by partial chemical substitution of Sm ions by non-magnetic trivalent ions (e. g. Y^{3+}, La^{3+}) [22,23]. The X-ray absorption near edge structure (XANES) measurements revealed that the introduction of vacancies in rare-earth sublattice increases the effective Sm valence while the lanthanum doping produces the opposite effect [25]. In terms of thermal expansion, a variation of effective Sm valence results in a shift of CTE minimum on the temperature scale and a change of its depth [22,23,26,27]. Summarizing the above, NTE of the IV systems can be adjusted using several methods. CTE of MMCs reinforced with the particles of IV compounds can be precisely tailored to a specific value depending upon the functional material in use and conditions of application. It should be emphasized that the flexibility in CTE control of the proposed MMCs is much higher than in the classical MMCs, in which the thermal expansion is only defined by the ratio of constituents volume fractions. The fundamental difference between composites based on IV systems and previously studied MMCs is the metallic nature of some IV NTE compounds, which appear better suited for modifying the properties of a metal matrix compared to ceramic NTE materials. The values of NTE in IV systems vary widely although the variation in temperature is limited. NTE values of selected IV systems are listed in Table 1 [28–32].

The temperature range over which the IV systems based on Sm and Yb display NTE imposes restrictions on the invar region of composites. Namely, one should expect operation at temperatures below room temperature. This limitation is not dramatic, since the operating temperatures of many applications, for example the aerospace or cryogenic technologies, lie mainly within the range of low temperatures.

Simple structural materials whose only advantages are mechanical properties and dimensional stability when heated or cooled are out of discussion. In turn we are trying to contribute to the progress in the development of materials with unique combinations of functional properties (electronic/ magnetic/ thermodynamic/ transport/ optical) with a specified limit on the CTE value.

This research explored the characterization of microstructure and thermal expansion behaviour of the first developed MMCs reinforced with the particles of an IV system. We aimed to decrease the CTE of Al, a widely used functional material, to near zero value at certain temperature by adding particles of classical IV system with NTE – SmB_6. Although the contraction of SmB_6 is not the highest among IV systems and is limited by low temperatures, the use of this compound as NTE filler can be beneficial due to its high chemical stability and high melting point, which prevent chemical reaction with the metal matrix. Another important point is the commercial availability of samarium hexaboride. Readers who are interested in higher temperatures or need larger NTE

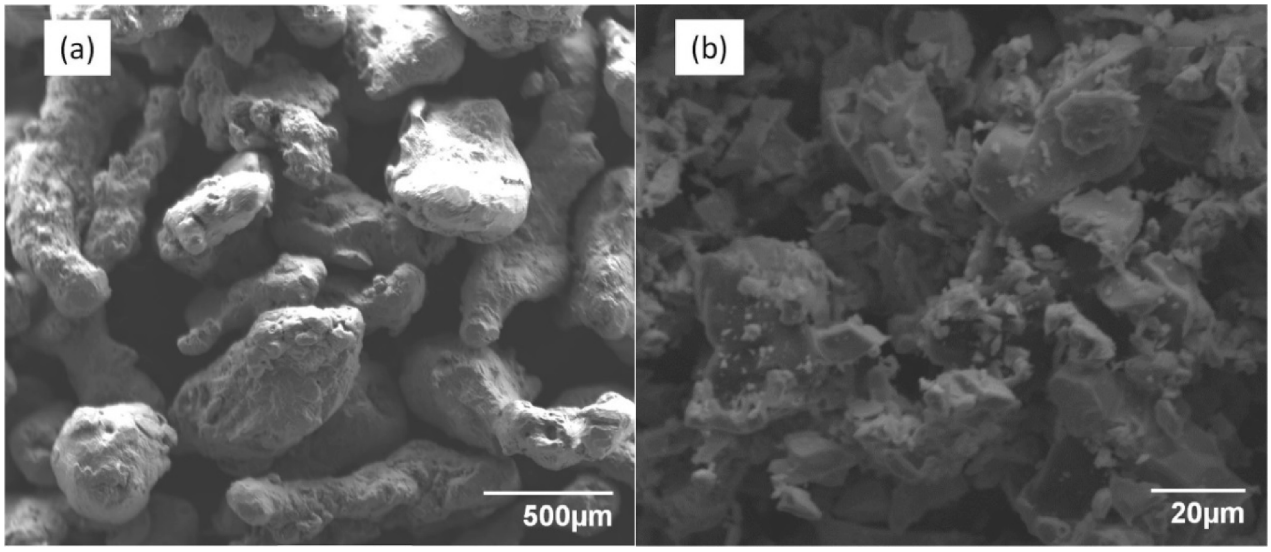

Fig. 1. SEM image of Al (a) and SmB_6 (b) powders.

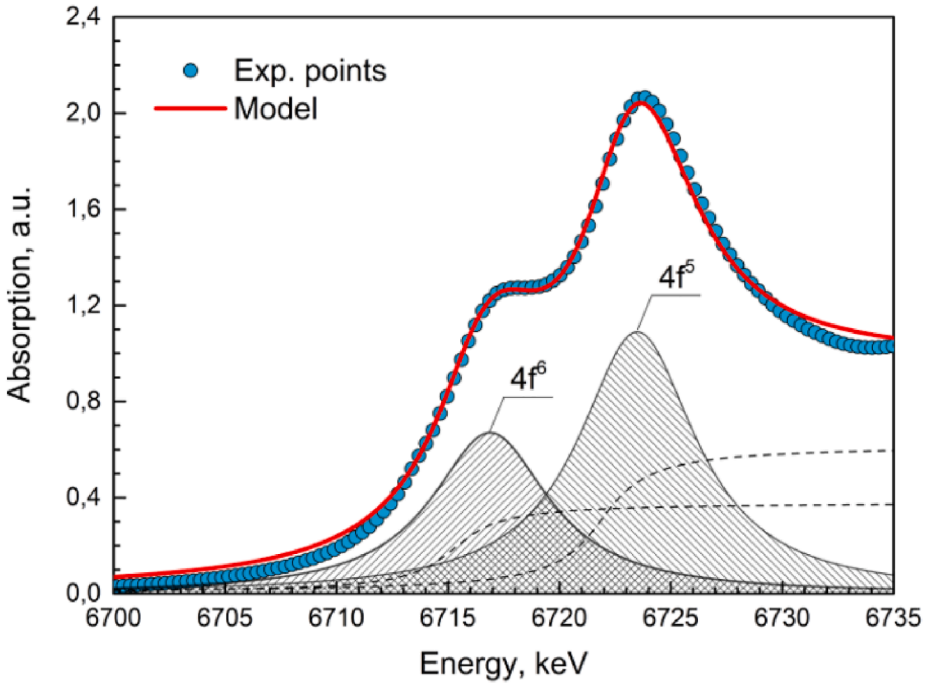

Fig. 2. Sm L_3-edge absorption spectra of SmB_6 at 300 K.

values can refer to Table I or review articles [17,19].

In this article, we would like to present the results of the study of Al/SmB_6 composite fabricated by hot pressing powder blends. The sample has been examined by optical and electron microscopy, X-ray tomography, and X-ray diffraction. Thermal expansion of Al/SmB_6 composite has been measured by capacitive dilatometry and analyzed using various theoretical models to single out the best model for CTE description in novel metal/metal composite.

Experimental methods and techniques

Composite preparation

Commercially available Al powder (UC Rusal, 99.5% purity, size < 0.5 mm) and SmB_6 powder (Haihang Industry Co., Ltd, 99.9% purity, size < 20 μm) were used for the study (Fig. 1a and b respectively). In the beginning, Al powder was ball milled in a PULVERISETTE 6 (Fritsch, Germany) planetary ball-mill through the use of ceramic ZrO_2 milling balls with a diameter of 8 mm and a ball-to-powder weight ratio of 15:1. Ball milling was carried out for 15 min with the revolving speed 400 rpm. After that SmB_6 powder were weighed and mixed with finely powdered aluminum with the mass ratios of 1:2, which corresponding to SmB_6-21 vol%. According to the Turner model this mass ratio meet a requirement of near zero CTE of Al/SmB_6 composite at T = 40 K, i.e. the temperature at which SmB_6 exhibits the largest NTE. Powder blend were then high-energy ball milled for 10 min under the same conditions. The resulting mixture of Al/SmB_6 powders was hot pressed in a special heated steel die at 450 °C under an applied pressure of 350 MPa to obtain a compact with a diameter of 17 mm and a height of 10 mm.

Characterization

The surface morphology of initial Al and SmB_6 powders, Al/SmB_6 powder blend and bulk composite was imaged using a JEOL JSM-6390LV scanning electron microscope (SEM).

The X-ray absorption near edge structure (XANES) measurements near the Sm L_3-edge were carried out for SmB_6 at the STM beamline of Kurchatov synchrotron radiation source KISI at room temperature to experimentally confirm the IV state of Sm ions. The Al and SmB_6 powders, Al/SmB_6 powder blend and Al/SmB_6 bulk composite were characterized by X-ray diffraction (XRD) using synchrotron-generated X-Ray beam with E = 15.2 keV (λ = 0.826 Å) at STM beamline of KISI source and using laboratory X-ray source BRUKER D8 ADVANCE with E = 8.04 keV (λ = 1.541 Å).

The distribution of SmB_6 particles within an Al matrix in the fabricated Al/SmB_6 composite was analyzed by optical microscopy (Leica DM ILM) on the polished surfaces. The microstructure of the entire volume of the sample was studied by X-ray computed tomography (Y. Cheetah YXLON X-ray inspection system). In contrast to classical methods for microstructure characterization, such as optical or electron microscopy, which require preliminary sample cutting, etching and polishing, X-ray tomography is a non-destructive tool for internal structure diagnostic of the entire volume of the sample. Using slice-to-slice technology X-ray computed tomography reconstructs 3D models from a set of 2D X-ray images with a high resolution (up to 2 μm).

Thermal expansion measurements of Al/SmB_6 composite were carried out at Kirensky Institute of Physics by capacitive dilatometry using a hand-made measuring cell/option installed in the PPMS (Quantum Design) system (for more details see [33]) in the temperature range 10–210 K.

Experimental results

XANES

The experimental spectrum in Fig. 2 displays two characteristic peaks corresponding to the integer valent states: divalent $4f^6$ state and trivalent $4f^5$ state of Sm atom.

The absorption line shapes were analyzed using a deconvolution technique presented in [34]. Using a set of Lorentzian and arctangent functions representing the core–hole lifetime width and the transitions into the continuum states respectively, we fit the following expression to the experimental spectrum:

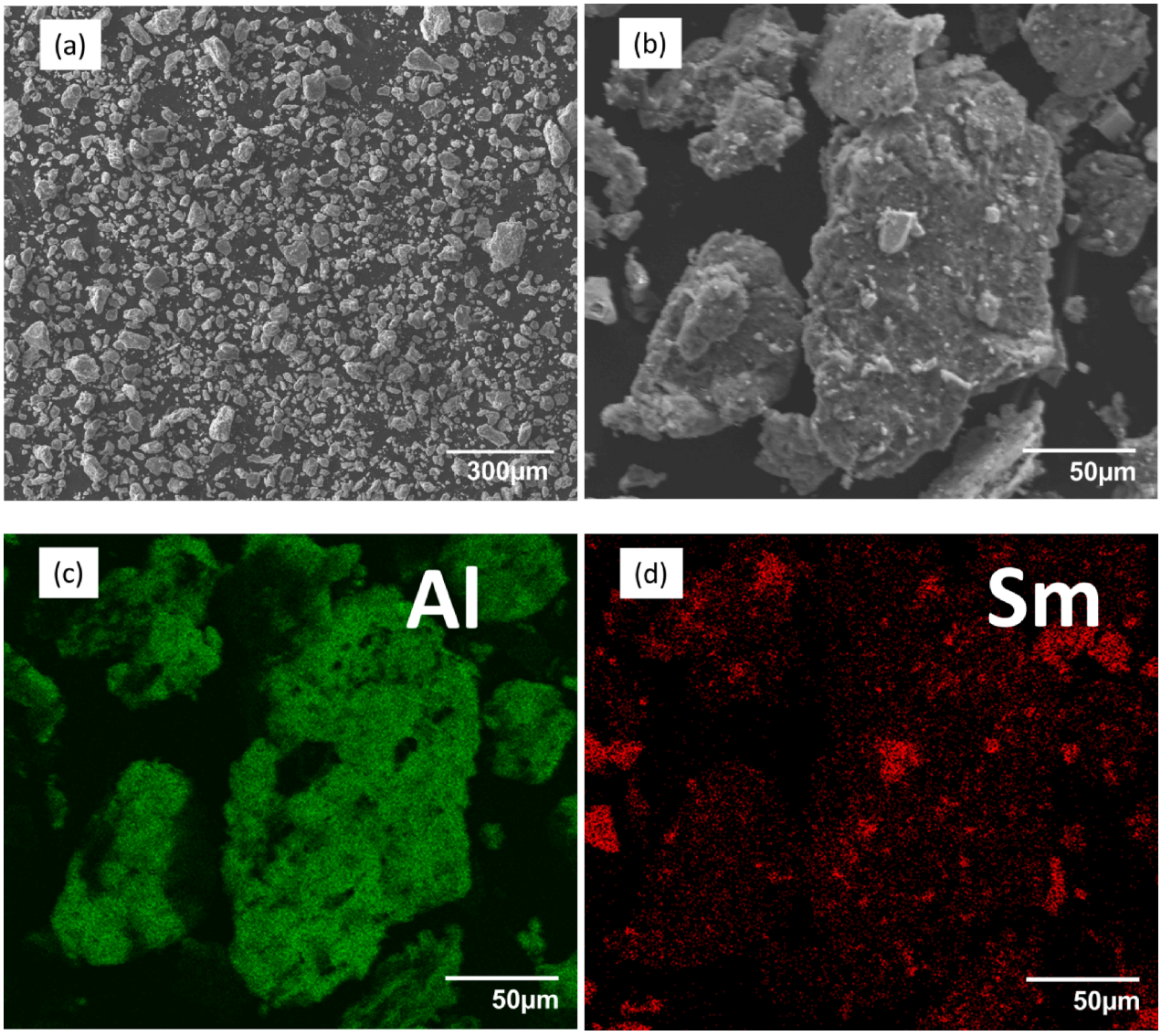

Fig. 3. SEM images of Al/SmB_6 powder blend (*a, b*) and EDS elemental mapping (*c, d*).

$$I(E) = B_0 + B_1 E + \sum_{k=1,2} \frac{p(k)\Gamma^2}{\Gamma^2 + (E - E_k)^2} + \sum_{c=1,2} \frac{p(c)}{p(1) + p(2)} \left(0.5 + \frac{1}{\pi} arctan \frac{E - E_c + \delta}{0.5\Gamma}\right) \quad (1)$$

Here E is the photon energy, B_0 and B_1 denote linear background. The strengths of the individual Lorentzian line shapes are given by p_1 and p_2, while a half-width at full maximum Γ denotes the lifetime of electron excitation from 2p-core level to an empty 5d-states. The δ value corresponds to a shift of the continuum of −1.6 eV as observed in Sm-based compounds [35]. As a result of fitting procedure we extracted the independent parameters $p_1 = 0.67$, $p_2 = 1.09$ and $\Gamma = 3.2$ eV. The ratio of amplitudes p_1/p_2, expressing the effective intermediate valence $Sm^{+2.61}$, is in a good agreement with that reported earlier for SmB_6 [36].

Microstructure and XRD

Fig. 3 shows the SEM images of Al/SmB_6 powder blend and EDS elemental mapping (the map for light B atoms is omitted since it's less indicative than the map for Sm atoms with high Z number). As can be seen from the Fig. 3a, the size of the particles doesn't exceed 150 μm.

The resulting mixture consists of Al + SmB_6 agglomerates and SmB_6 particles (Fig. 3b,c,d). Agglomerates present micro- and sub-micron particles of samarium hexaboride embedded in aluminum matrix. Agglomerates are characterized by an irregular shape with a developed surface morphology. In contrast, SmB_6 particles can be identified by the smooth chipping surfaces, typical of brittle materials.

Typical optical micrographs of Al/SmB_6 bulk composite are depicted in Fig. 4a,b. The results indicate that samarium hexaboride particles are dispersed homogeneously within the aluminum matrix and their size doesn't exceed 20 μm. Negligible pores with a size less than 5 μm are also observed in Fig. 4a, formation of which usually accompanies the

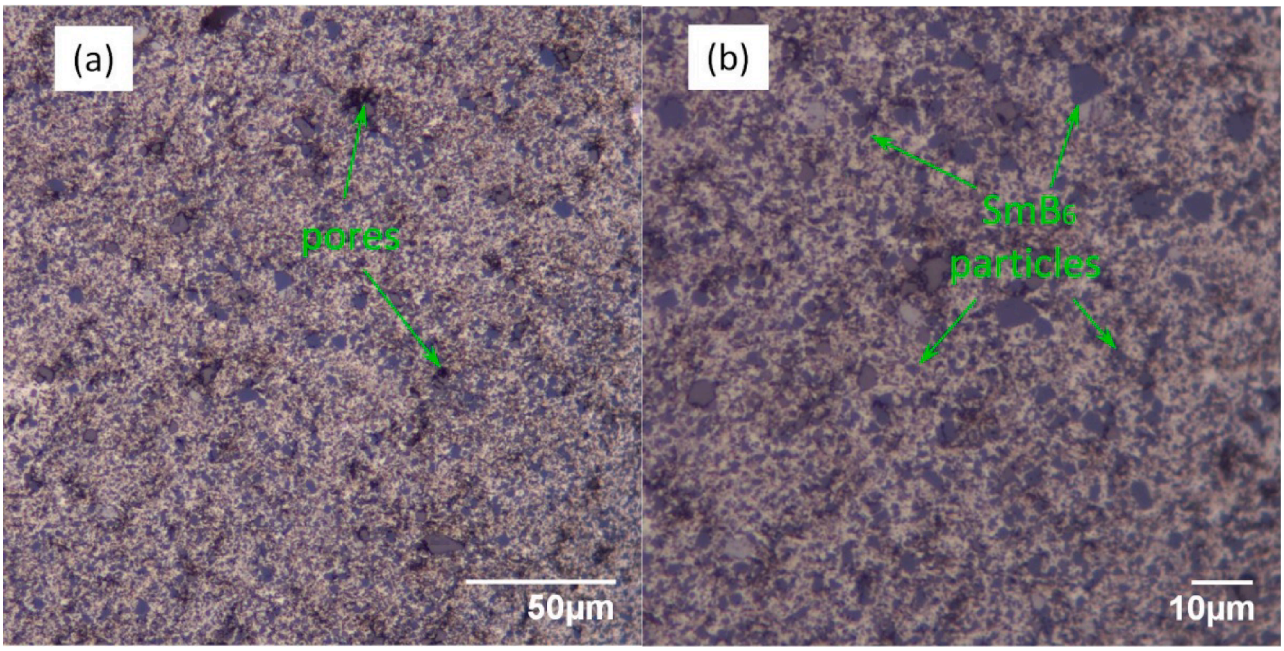

Fig. 4. Optical micrographs of Al/SmB_6 composite.

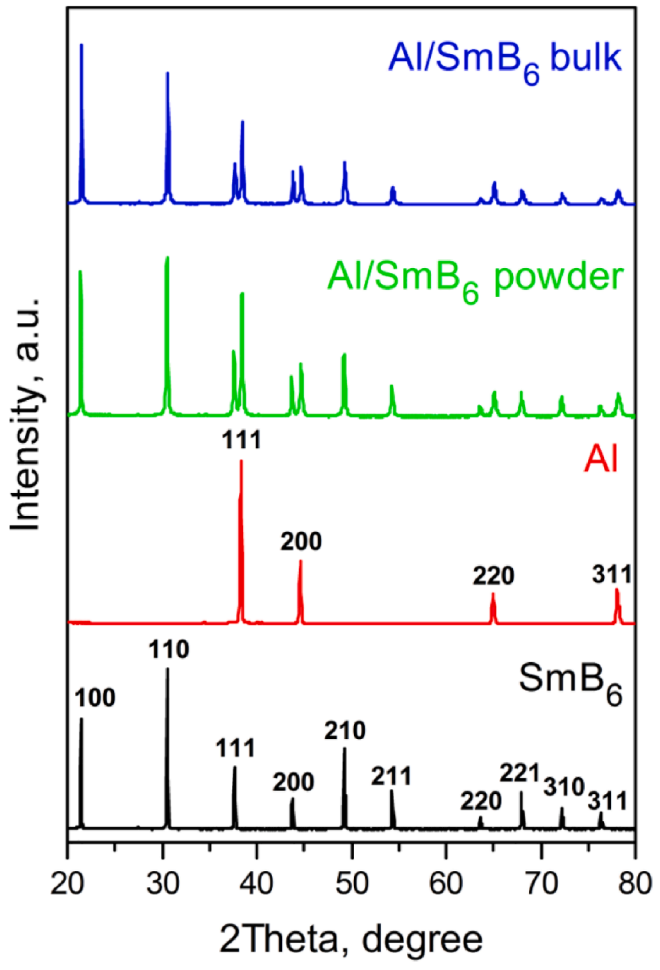

Fig. 5. XRD patterns of Al and SmB_6 powders, Al/SmB_6 powder blend and Al/SmB_6 composite.

polishing procedure. It should be noted that some pores may have remained after the pressing process, nevertheless their size and volume fraction are negligible and can't affect the thermodynamic properties of the sample significantly.

The XRD patterns of Al and SmB_6 powders, Al/SmB_6 powder blend and Al/SmB_6 bulk composite are presented in Fig. 5.

The XRD study confirms *Fm-3 m* (№ 225) space group of Al and *Pm-3 m* (№ 221) space group of SmB_6 and indicates the absence of any other crystal structures. In turn, XRD patterns of Al/SmB_6 powder blend and bulk composite are fully defined by peaks attributed to Al and SmB_6 thereby indicating that no chemical reactions occurred to form novel phases.

Fig. 6 shows 3D model of Al/SmB_6 composite reconstructed based on the results of X-ray computed tomography. In addition, Fig. 6 includes X-ray 2D-sections in three basic planes indicated in a 3D model. A full scan along the pressing axis (a set of 2D-images at different lengths) is available in Supplementary materials.

X-ray tomographic analysis revealed a homogeneous structure of the composite at the macro scale, while a uniform distribution of SmB_6 particles within an Al matrix at the micro scale was confirmed by optical microscopy (Fig. 4). For comparison, we present X-ray cross-section of other composite manufactured using a different technology (Fig. 7). As can be seen from the image, a granular structure has formed near one of the two plane-parallel faces of the sample probably due to powders segregation at the mixing stage.

From the above, it can be inferred that the manufacturing route and the process conditions for a fabrication of the composite under consideration were selected properly.

Coefficient of thermal expansion

The relative thermal expansion of Al/SmB_6 composite measured by capacitive dilatometry using a hand-made measuring cell/option installed in the PPMS (Quantum Design) system is shown in Fig. 8a.

Since the cell material also expands upon heating, this contribution to thermal expansion was defined and extracted through the capacitance measurements of silver with 99.99% purity, the CTE values of which are well known [37,38]. It's worth noting that we performed repeated measurements, which showed identical results, to make sure that a

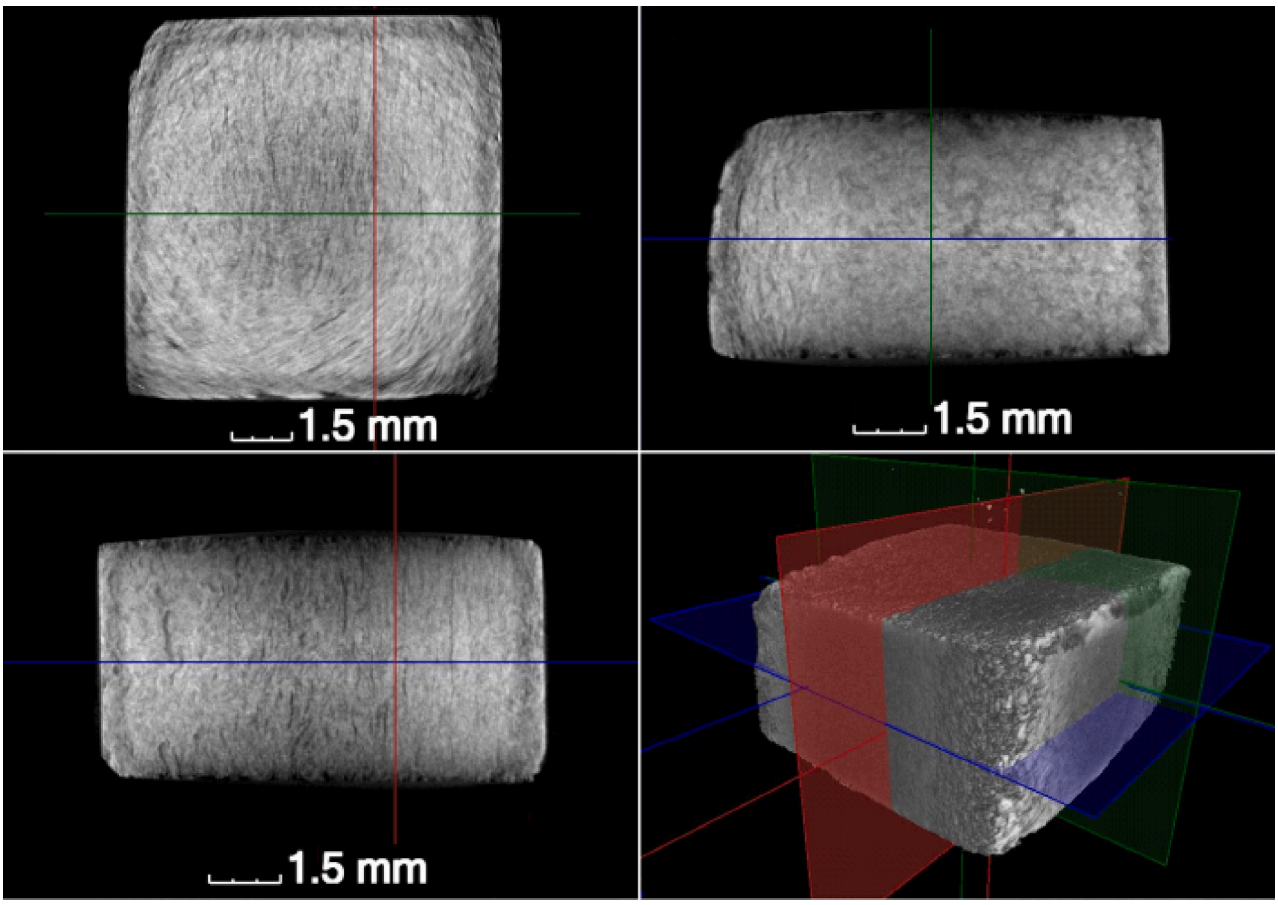

Fig. 6. X-ray 2D-sections in three basic planes and a 3D X-ray micro tomographic reconstruction of Al/SmB_6 composite. Color palette is inverted, i.e. the black color indicates the regions without absorption of X-rays.

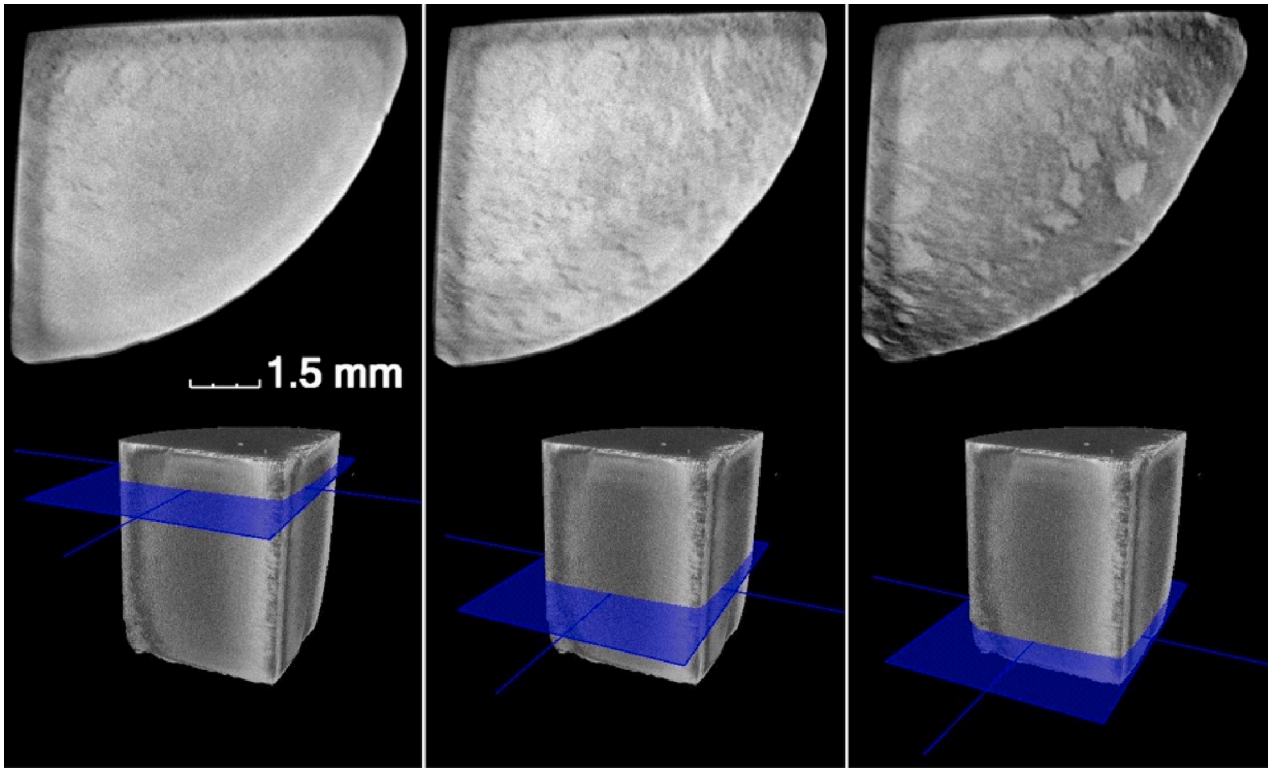

Fig. 7. X-ray cross-sections at varying heights of the second Al/SmB_6 composite manufactured using a different technology.

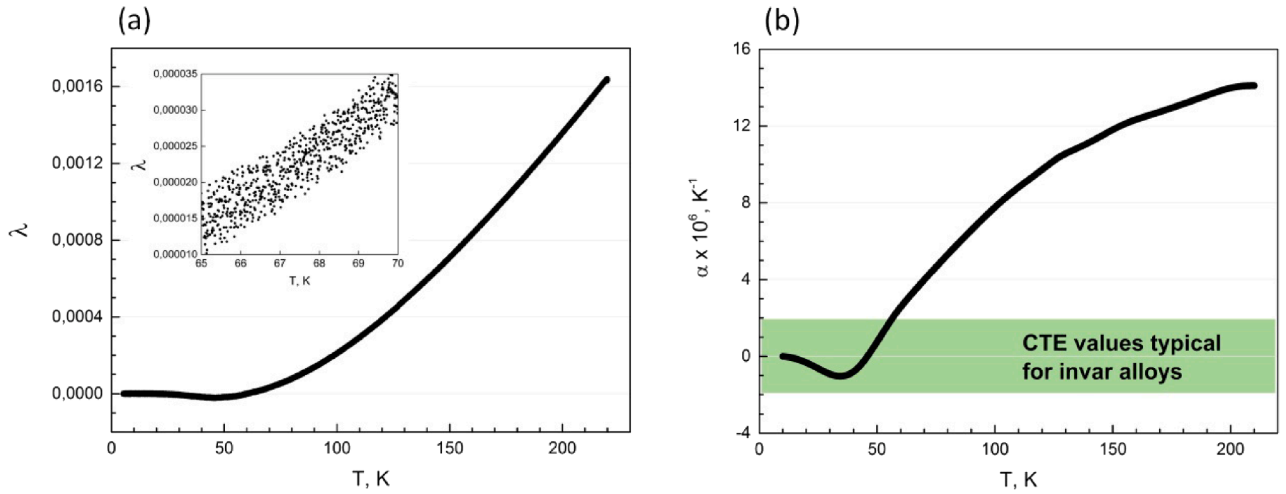

Fig. 8. Relative thermal expansion (a) and linear CTE (b) of Al/SmB_6 composite in the temperature range 10–210 K. The inset indicates a spread of values.

probable stress relaxation doesn't affect the experimental curve (such physical picture was observed in [13] for example).

In Fig. 8b we show the experimental results of the linear CTE of Al/SmB_6 composite obtained by taking derivatives $d\lambda/dT$. To prevent oscillations of the CTE function, the dependence $\lambda(T)$ were preliminarily smoothed using the spline function. Below ~45 K, α is negative, while at higher temperatures α then becomes positive. Filled area on Fig. 8b indicates that the sample exhibits invar behaviour, i.e. CTE values less than $|2| \times 10^{-6}\,K^{-1}$, at temperatures up to ~60 K. In comparison to pure aluminum, the temperature range has increased by about 20 K.

The temperature range of invar-like behaviour (0–60 K) may seem rather narrow for practical applications. In particular, it is lower than the boiling point of liquid nitrogen T = 77 K, which closes many potential niches for the developed material. In our case, we are not trying to compete with classical Fe-Ni alloys in their well-known application. On the contrary, the motivation was to develop invar materials of a new type and test the principle. For instance, the thermal conductivity of classic Fe-Ni36 invar alloy is almost 20 times lower comparing to pure aluminum [39]. In this way, the developed Al/SmB_6 composite may possesses a unique combination of useful functional properties inherent in the matrix material, and a specified limit on the CTE value.

Discussion

To develop composites with predetermined properties, such as the thermal expansion, it is very important to base on a reliable model capable of predicting CTE of the composite. Those models that worked well for ceramic-based MMCs may be less efficient for the systems under study. The point is that SmB_6, the compound that belongs to the class of higher borides, differs greatly in its physical properties from complex oxides and ceramic materials. The composites studied in this work can be considered as systems based on metal components excepting the region of the lowest temperatures. Pure SmB_6 is a narrow-gap insulator (Kondo insulator), but at temperatures above several tens of degrees, the electrical conductivity becomes metallic. Any inhomogeneities and impurities reduce the size of the gap in the density of the electronic states of

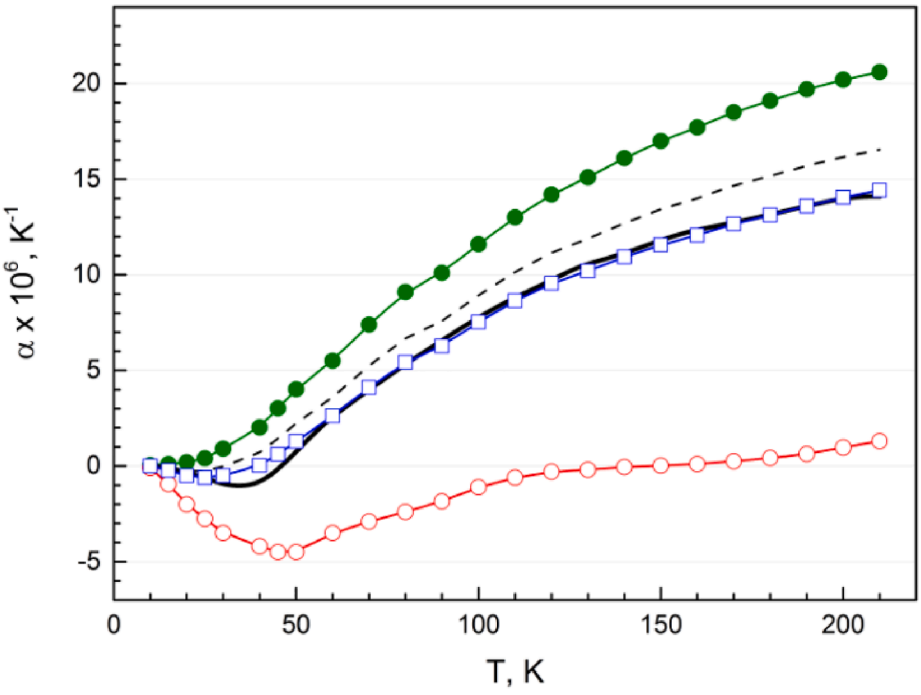

Fig. 9. Plot of experimental CTE values (black solid line) along with curves representing CTE values calculated using thermo-elastic models for the Al/SmB_6 composite. Green filled circles – CTE of Al; red open circles – CTE of SmB_6; dashed line – results of the ROM model assuming SmB_6-21 vol%; blue open squares – results of the ROM, Terner and Kerner models assuming various volume fractions, see text for details. (For interpretation of the references to color in this figure legend, the reader is referred to the web version of this article.)

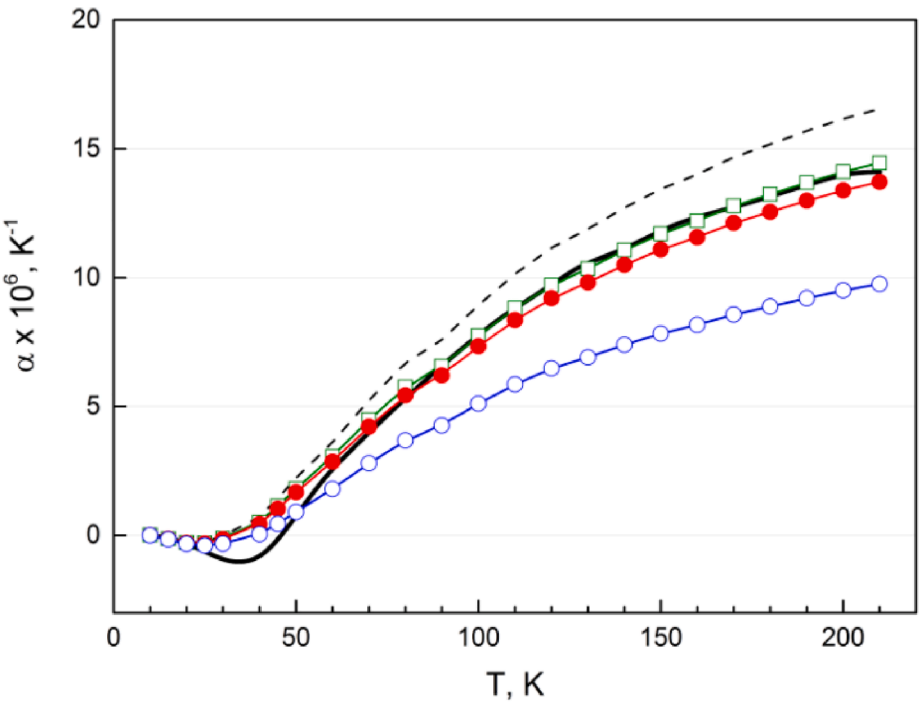

Fig. 10. Plot of experimental CTE values (black solid line) along with curves representing CTE values calculated using the EROM model for the Al/SmB_6 composite N°1. Dashed line – results of the classic ROM model assuming SmB_6-21 vol%. Symbols – results of the EROM model assuming: $\alpha_{in} = \alpha_{Al}/3$ and $\Delta = 2$ μm (green squares), $\alpha_{in} = \alpha_{Al}/10$ and $\Delta = 2$ μm (red filled circles), $\alpha_{in} = \alpha_{Al}/10$ and $\Delta = 4$ μm (blue open circles). (For interpretation of the references to color in this figure legend, the reader is referred to the web version of this article.)

this system, since the mechanism for forming this gap is based on cooperative phenomena and coherence in the samarium sublattice. At elevated temperatures, commercially available samarium hexaboride is similar to good metals in terms of transport properties, although it has a noticeably higher hardness. We will leave these questions to the domain of condensed matter physics. Coming back to the context of material science problems of novel composites, much attention should be paid to the comparison of models focused on quantitative analysis of experimental results presented in the previous section.

The simplest approach is the rule of mixtures (ROM) (2):

$$\alpha_c = \alpha_f \nu_f + \alpha_m \nu_m \tag{2}$$

where the subscripts c, f and m denote the composite, filler and matrix respectively; α – CTE; υ – volume fraction. More sophisticated treatments are based on widely used Turner (3) and Kerner (4) models:

$$\alpha_c = \left(\alpha_f \upsilon_f K_f + \alpha_m \upsilon_m K_m\right) / \left(\upsilon_f K_f + \upsilon_m K_m\right) \tag{3}$$

$$\alpha_c = \alpha_m \upsilon_m + \alpha_f \upsilon_f + \upsilon_m \upsilon_f \left(\alpha_f - \alpha_m\right) \frac{K_f - K_m}{\upsilon_m K_m + \upsilon_f K_f + 3K_m K_f / 4G_m} \tag{4}$$

where K – bulk modulus; G – shear modulus [40].

In the following part we analyze the dilatometric experimental data based on the thermo-elastic models given by Eqs. (2)–(4). In our calculations we used literature values for the bulk properties of Al and SmB_6 as long as the size of the particles lies in the range of microns and sub-microns. In particular, we used the thermal expansion data for Al [41] SmB_6 [22] and their elastic properties: $K_{SmB6} = 136$ GPa [42] $K_{Al} = 78.88$ GPa [39] $G_{Al} = 25.5$ GPa [43]. A comparison of experimental and computed data is depicted in Fig. 9.

As can be seen from Fig. 9, the CTE values predicted by the ROM model are significantly higher than the experimental ones. Near perfect fit is provided by the Terner model (blue open squares in Fig. 9). The same results can be obtained within the ROM model or the Kerner model through the use of increased SmB_6 volume fraction: SmB_6-32 vol% and SmB_6-29 vol% respectively. It should be noted that the size of originally manufactured composite was too big for the thermal expansion measurements, therefore the smaller piece was cut off with a form shown in Fig. 6. As a consequence, there is a low probability that the volume fractions of Al and SmB_6 powders at local sites of the composite may deviate from the expected SmB_6-21 vol% by a certain amount. However, since the composite's microstructure is almost homogeneous, we are of the opinion that the volume ratio is close to the expected SmB_6-21 vol%. From the above we can assert that the Turner model provides a more accurate assessment.

At the end we attempted to describe the thermal expansion data with the extended ROM (EROM) model fully described in [44,45]. Unlike the classic ROM this approach takes into account the size of the filler particles, which is known rather well in our case. The heart of the method involves identifying an entire composite as the sum of an elastic matrix region, spherically symmetric elastic particle region and an interfacial elasto-plastic matrix region (5):

$$\alpha_c = \alpha_f \nu_f + \alpha_{in} \nu_{in} + \alpha_m \nu_m \tag{5}$$

where the subscript *in* denotes interfacial region. Taking into account a spherical symmetry of the particles Eq. (5) can be expressed as follows (6):

$$\alpha_c = \alpha_f \nu_f + \alpha_{in} \nu_f \left[\frac{(R+\Delta)^3}{R^3} - 1\right] + \alpha_m \left(1 - \nu_f \frac{(R+\Delta)^3}{R^3}\right) \tag{6}$$

where R – radius of the particle; Δ - width of the interfacial region.

An estimation of the filler particle size was performed through the use of combination of sieve analysis and optical/electron microscopy. During the sieve analysis the particles passed through a series of sieves with progressively smaller mesh size: 80 μm, 50 μm and 20 μm. The results of analysis indicate that the particles size do not exceed 20 μm. This is confirmed by microscopy examination presented in Figs. 3 and 4. Thus, we used $R = 10$ μm in Eq. (6). As for the fitting parameters α_{in} and Δ, their initial values were chosen arbitrarily based on the following assumptions: Δ is smaller than R, α_{in} is proportional to α_m as long as filler particles are considered perfectly elastic. The outcome of calculations for the Al/SmB_6 composite is depicted in Fig. 10.

Fig. 10 shows that the best fit obtained within the EROM model (green squares) describes the experimental curve well in the temperature range 60–210 K, however at lower temperatures it's far from being

perfect. From this point, the Turner model provides a better match in total. Variation of α_{in} and Δ values, as well as R, doesn't improve the CTE fit below 60 K, however, it significantly increases the discrepancy between theoretical and experimental data at higher temperatures (see Fig. 10).

As shown in this section, the Turner model is well-suited for CTE description of Al/SmB_6 composite over a very wide temperature range. We assume that it will remain reliable for the composites based on doped (modified) samarium hexaboride. However, this assumption should be confirmed by the forthcoming studies. It should be noted that we relied on literature data on the elastic properties of SmB_6. In the case of doped borides, in order to use the Turner model one should either measure the elastic properties of the IV component or use model assumptions on the value of the bulk modulus.

Conclusions

In this work, the microstructure and the thermal expansion behaviour of the metal matrix composite based on the intermediate valence system were experimentally studied for the first time. Using the hot-pressing method we fabricated a composite comprising Al-79 vol%, a widely used functional material, and SmB_6-21 vol%, a classical intermediate valence system with negative thermal expansion. In contrast to ceramic NTE fillers like ZrW_2O_8, the values of negative thermal expansion in intermediate valence systems can be varied either by introducing vacancies in the rare-earth sublattice or by partial chemical substitution of 4f-elements with partially filled electron shells by non-magnetic analogue with an integer valence state. From this perspective, intermediate valence systems with NTE are better suited for modifying the thermal expansion of a metal matrix compared to ceramics with strictly specified NTE values.

The Al/SmB_6 composite was characterized by XRD, optical and electron microscopy, X-ray computed tomography. Using the latter technique 3D volumetric model showing SmB_6 particles distribution within an Al matrix was reconstructed. The measurements of thermal expansion carried out by capacitive dilatometry revealed that the sample exhibits invar behaviour, i.e. CTE values less than $|2| \times 10^{-6}\,K^{-1}$, up to ~60 K with a zero value of coefficient of thermal expansion near 45 K. In comparison to pure aluminum, the temperature range has increased by about 20 K. A quantitative analysis of dilatometric experimental data performed on the basis of widely used theoretical models showed that the thermal expansion Al/SmB_6 composite was well reproduced within the Turner model.

CRediT authorship contribution statement

D.A. Serebrennikov: Investigation, Writing - original draft. **A.A. Bykov:** Investigation, Writing - review & editing. **A.L. Trigub:** Investigation. **N.A. Kolyshkin:** Investigation, Writing - review & editing. **A.L. Freydman:** Investigation, Writing - review & editing. **A.V. Aborkin:** Investigation, Writing - original draft. **A.O. Tovpinets:** Investigation, Writing - review & editing. **E.S. Clementyev:** Conceptualization, Writing - original draft. **A.Yu. Goikhman:** Supervision, Funding acquisition, Writing - review & editing.

Declaration of Competing Interest

The authors declare that they have no known competing financial interests or personal relationships that could have appeared to influence the work reported in this paper.

Acknowledgements

This work was supported by the Russian Foundation for Basic Research, grant 18-32-00583 mol_a and by the State assignment of Russia, project FZWM-2020-0008. We are grateful to V.N. Leitsin for his support in the experimental studies.

Appendix A. Supplementary data

Supplementary data to this article can be found online at https://doi.org/10.1016/j.rinp.2021.103843.

References

[1] Wasserman EF. Acet M. Invar, Anti-Invar: Magnetovolume Effects in Fe-Based Alloys Revisited. In: Planes A., Manosa L., Saxena A., editors. Magnetism and Structure in Functional Materials. Berlin, Heidelberg: Springer, 177; 2005.
[2] Shiga M. Curr Opin Solid State Mater Sci 1996;1:340.
[3] Wasserman EF. INVAR: Moment-volume instabilities in transition metals and alloys. In: Buschow, K. H. J. &Wohlfarth, E., editors. Ferromagnetic Materials Vol. 5. Amsterdam: North-Holland, 237; 1990.
[4] Schilfgaarde M, Abrikosov IA, Johansson B. Lett Nat 1999;400:46.
[5] Sidhu SS, Kumar S, Batish A. Crit Rev Solid State Mater Sci 2016;41:132.
[6] Wu D, Wu S-P, Yang L, Shi C-D, Wu Y-C, Tang W-M. Powder Metall 2015;58:100.
[7] Nam TH, Requena G, Degischer P. Compos A 2008;39:856.
[8] Shu K-M, Tu GC. Mater Sci Eng, A 2003;349:236.
[9] Xue ZW, Wang LD, Liu Z, Fei WD. Scr Mater 2010;62:867.
[10] Elomari S, Skibo MD, Sundarrajan A, Richards H. Compos Sci Technol 1998;58:369.
[11] Ibrahim IA, Mohamed FA, Lavernia EJ. J Mater Sci 1991;26:1137.
[12] Mary TA, Evans JSO, Vogt T, Sleight AW. Science 1996;272:90.
[13] Holzer H, Dunand DC. J Mater Res 1999;14:780.
[14] Gao S, Zhao N, Liu Q, et al. J Alloys Compd 2019;779:108.
[15] Sa Das, Si Das, Das K. Ceram Int 2014;40:6465.
[16] Sleight AW. Ann Rev Mater Sci 1998;28:29.
[17] Chen J, Hu L, Deng J, Xing X. Chem Soc Rev 2015;44:3522.
[18] Evans JSO. J Chem Soc, Dalton Trans 1999;19:3317.
[19] Barrera GD, Bruno JAO, Barron THK, Allan NL. J Phys: Condens Matter 2005;17:R217.
[20] Takenaka K. Sci Technol Adv Mater 2012;13:013001.
[21] Riseborough RS, Lawrence JM. Rep Prog Phys 2016;79:084501.
[22] Nefedova EV, Alekseev PA, Klement'ev ES, Lazukov VN, Sadikov IP, Khlopkin MN, Tsetlin MB, JETP 88, 565; 1999.
[23] Alekseev PA, Mignot J-M, Nefeodova EV, et al. Phys Rev B 2006;74:035114.
[24] Arvanitidis J, Papagelis K, Margadonna S, Prassides K, Flitch AN. Nature 2003;425:599.
[25] Gabani S, Flachbart K, Bednarcik J, Welter E, Filipov V, Shitsevalova N. Acta Phys Pol A 2014;126:338.
[26] Nefedova EV, Alekseev PA, Lazukov VN, Sadikov IP. JETP 2003;96:1113.
[27] Serebrennikov DA, Clementyev ES, Alekseev PA. J Magnetism Magnetic Mater 2019;470:131.
[28] Margadonna S, Arvanitidis J, Papagelis K, Prassides K. Chem Mater 2005;17:4474.
[29] Kuznetsov AYu, Dmitriev VP, Bandilet OI, Weber H-P. Phys Rev B 2003;68:064109.
[30] Hauser R, Ishii T, Uwatoko Y, Oomi G, Bauer E, Gratz E. JMMM 1996;157/158:679.
[31] Pott R, Schefzyk R, Wohlleben D, Junod AZ. Phys B - Condensed Matter 1981;44:17.
[32] Uwatoko Y, Oomi G, Thompson JD, Canfield PC, Fisk Z. Phys B 1993;186–188:594.
[33] Freidman AL, Popkov SI, Semenov SV, Turchin PP. Tech Phys Lett 2018;44:123.
[34] Rohler J. JMMM 1985;47&48:175.
[35] Deen PP, Braitwaite D, Kernavanois N, et al. Phys Rev B 2005;71:245118.
[36] Mizumaki M, Tsutsui S, Iga F. J Phys Conf Ser 2009;176:012034.
[37] White GK, Collins JG. J Low Temp Phys 1972;7:43.
[38] Küchler R, Bauer T, Brando M, Steglich F. Rev Sci Instrum 2012;83:095102.
[39] Babichev AP, Babushkina NA, Bratkovskiy AM, et al., In: Grigorieva I.S., Mejlihova E.Z., editors. Physical values. Moscow: Energoatomizdat, 1232; 1991.
[40] Hsien CL, Tuan WH. Mater Sci Eng, A 2007;460–461:453.
[41] Kozhevnikov IG, Novitskiy LA. In: Gordov A.N., editor. Teplofizicheskie svoistva materialov pri nizkih temperaturah. Moscow: Mashinostroenie, 98; 1982.
[42] Nakamura S, Goto T, Kunii S, Iwashita K, Tamaki A. J Phys Soc Jpn 1994;63:623.
[43] Archer RR, Cook NH, Crandall SH. et al. In: Clark BJ, editor. An introduction to the mechanics of solids. New York: McGraw-Hill Inc.; 1978. p. 286.
[44] Park C-S, Kim M-H, Lee C. J Mat Sci 2001;36:3579.
[45] Gonzalez-Benito J, Castillo E, Caldito JF. Eur Polym J 2013;49:1747.